

Tunable anisotropic magnetism in trapped two-component Bose gases

Yongqiang Li^{1,2}, M. Reza Bakhtiari¹, Liang He¹, Walter Hofstetter¹

¹*Institut für Theoretische Physik, Johann Wolfgang Goethe-Universität, 60438 Frankfurt/Main, Germany*

²*Department of Physics, National University of Defense Technology, Changsha 410073, P. R. China*

(Dated: June 29, 2018)

We theoretically address magnetic ordering at zero and finite temperature in both homogeneous and trapped Bose-Bose mixtures in optical lattices. By using Bosonic Dynamical Mean-Field Theory, we obtain the phase diagram of the homogeneous two-component Bose-Hubbard model in a three-dimensional (3D) cubic lattice, which features competing magnetic order of XY-ferromagnetic and anti-ferromagnetic type in addition to the Mott and superfluid states. We show that these magnetic phases persist also in the presence of a harmonic trap.

PACS numbers: 67.60.Bc, 67.85.Hj, 67.85.Fg

I. INTRODUCTION

Quantum magnetism is one of the most intriguing areas in condensed-matter physics. Even though the attempts to understand it root back to the early days of quantum theory, still there are many open questions even at the level of the minimalistic Hubbard model [1]. Many theoretical and experimental efforts have been devoted to revealing the mechanisms behind magnetic ordering of many-body systems [2]. Due to the high level of complexity in solid-state systems, a quantitative comparison between theory and experiment seems a very challenging task, if not impossible at all. Therefore it is highly desirable to work with systems which are able to *simulate* the original solid-state many-body systems, but in a much more controllable way.

Over the past decade cold-atomic quantum gases in optical lattices have provided an excellent laboratory for investigating many-body quantum systems with an unprecedented level of precision and control. Nowadays one can routinely create optical lattices with different geometries that mimic solid-state crystalline structures and then load different quantum gases into them, playing the role of electrons. Based on this experimental progress, fundamental many-body phenomena such as the Mott insulator quantum phase transition of interacting bosons have been realized [3]. For bosonic gases in optical lattices correlated atom tunneling [4] and superexchange due to second-order atom tunneling [5] have been observed, which are the basic mechanisms leading to quantum magnetism. At the current stage, detecting anti-ferromagnetic long-range ordering of spinful fermions or bosons is arguably the most challenging goal and there are large experimental and theoretical efforts directed towards reaching this phase. This may eventually give insights into the mechanism of high- T_c superconductivity as well [6]. The recently developed optical quantum gas microscope [7, 8] offers the possibility to detect quantum magnetism on the single-atom level, and has been utilized to observe the phase transition of a one-dimensional chain of interacting Ising spins by using a Mott insulator of spinless bosons in a tilted optical lattice [9].

In parallel to these experimental developments, there

are several theoretical proposals how to gain fundamental insight into quantum magnetism via ultracold gases [10–19]. One of the aims has been to realize a spin Hamiltonian by interacting ultracold bosons [10, 11]. For this two-component Bose gas in an optical lattice, which is effectively described by the Bose-Hubbard model, the complete phase diagram was mapped out by a variational approach [12].

A related important experimental achievement is given by mixtures of different quantum gases, whether with different statistics (Bose-Fermi mixture) or different isotopes of the same type (Bose-Bose or Fermi-Fermi mixture). Recently a Bose-Bose mixture of ⁸⁷Rb and ⁴¹K in a 3D optical lattice has been realized [20]. Here it is possible to tune independently the inter-species and intra-species interactions. In a follow-up experiment the same Bose-Bose mixture has been used to investigate the entropy exchange between two spin-dependent traps though without lattice [21]. Another Bose-Bose mixture, made of two hyperfine states of ⁸⁷Rb, has served as a spin gradient thermometer which allows to measure the temperature of ultra-cold atoms in optical lattices [22, 23]. In a further experiment the effect of the Bose-Bose inter-species interaction on the bosonic superfluidity of one of the components in a 3D optical lattice has been explored [24].

Motivated by these experiments, here we theoretically investigate a two-component Bose gas in 2D and 3D optical lattices. This system can be effectively modeled by the Bose-Hubbard model. We will specifically consider the case of filling $n = 1$ and $n = 2$ per site. We investigate the homogeneous (untrapped) system by means of Bosonic Dynamical Mean-Field Theory (BDMFT) [25–29] and the harmonically trapped case by its real-space generalization (RBDMFT), which extends the original BDMFT formalism to the study of inhomogeneous systems. DMFT has been established as a powerful tool for strongly-correlated fermionic systems [31], while BDMFT has recently been shown to provide a qualitatively and in 3D even quantitatively accurate picture of the Bose-Hubbard model [29]. For the homogeneous system, we extend our previous BDMFT analysis to higher filling $n = 2$ and a different set of interac-

tion parameters motivated by experiments. We map out the phase diagram and obtain diverse phases such as superfluid, unordered Mott state and XY-ferromagnetic order. In addition we turn to the inhomogeneous (trapped) Bose-Hubbard model which is more closely related to the experimental situation. We include the effect of the external confining potential by RBDMFT, which assumes site-dependent self-energies. In parallel we perform also a complementary calculation based on a Local Density Approximation (LDA) combined with BDMFT which is computationally more affordable. Comparing results of both methods, we examine the magnetic properties of the system for a wide range of parameters. To our best knowledge this is the first systematic and non-perturbative study of the magnetic properties of a two-component inhomogeneous Bose-Hubbard model. It will bring more insight into ongoing experiments on Bose-Bose mixtures in optical lattices.

The paper is organized as follows: in section II we give a detailed description of the RBDMFT approach. Section III covers our results for the homogeneous Bose-Hubbard model. In Section IV we consider the trapped system and present results by RBDMFT and LDA+BDMFT. We summarize with a discussion in Section V.

II. MODEL AND METHOD

We consider a two-component bosonic mixture in an optical lattice with either 2D square or 3D cubic geometry. Experimentally the Bose-Bose mixture could consist of two different species, *e.g.* ^{87}Rb and ^{41}K as in Ref. [20] or two different hyperfine states of a single species, *e.g.* ^{87}Rb as in Refs. [5, 22, 24]. In addition we include an external harmonic trapping potential which gives rise to inhomogeneity. This system can be described by a two-component inhomogeneous Bose-Hubbard model

$$\begin{aligned} \mathcal{H} = & - \sum_{\substack{\langle i,j \rangle \\ \nu=b,d}} t_\nu (b_{i\nu}^\dagger b_{j\nu} + h.c) + \frac{1}{2} \sum_{i,\lambda\nu} U_{\lambda\nu} \hat{n}_{i,\lambda} (\hat{n}_{i,\nu} - \delta_{\lambda\nu}) \\ & + \sum_{i,\nu=b,d} (V_i - \mu_\nu) \hat{n}_{i\nu} \end{aligned} \quad (1)$$

In this Hamiltonian $\langle i, j \rangle$ represent the nearest neighbor sites i, j and we denote the two bosonic species as b, d which are labeled by the index $\lambda(\nu) = b, d$. The bosonic creation (annihilation) operator for species ν at site i is $b_{i\nu}^\dagger$ ($b_{i\nu}$) and the local density is $\hat{n}_{i,\nu} = b_{i\nu}^\dagger b_{i\nu}$. Due to possibly different masses or a spin-dependent optical lattice, these two species in general hop with non-equal amplitudes t_b and t_d . $U_{\lambda\nu}$ denotes the inter- and intra-species interactions, which can be tuned via a Feshbach resonance or by spin-dependent lattices. μ_ν denotes the global chemical potential for the two bosonic species and V_i the harmonic trap.

For the fermionic Hubbard model, DMFT has been developed and implemented successfully [30, 31] as a non-

perturbative formalism to study strongly-correlated electronic systems. This includes real-space generalizations of DMFT to address inhomogeneous fermionic systems [32, 33]. In spite of this success, a bosonic version of DMFT (BDMFT) for the Bose-Hubbard model has been formulated [25] and implemented [26, 27, 29] only very recently. Inspired by the case of fermions, here we extend BDMFT [26] to a real-space BDMFT (RBDMFT) formalism for inhomogeneous systems to include also the harmonic trap which is crucial in the experiments. RBDMFT is capable of providing an accurate and non-perturbative description of the ground-state of the inhomogeneous Bose-Hubbard model (1). Like fermionic DMFT, also BDMFT assumes that the self-energy of the system is local. However, in an inhomogeneous system it depends on the lattice site, *i.e.* $\Sigma_{\lambda\nu}^{(i,j)} = \Sigma_{\lambda\nu}^{(i)} \delta_{i,j}$ where $\delta_{i,j}$ is a Kronecker delta.

In a more formal language, first we map the Hamiltonian (1) onto a set of individual single-site problems each of which is described by a *local* effective action

$$\begin{aligned} S_{\text{eff}}^{(i)} = & \int_0^\beta d\tau d\tau' \sum_{\lambda,\nu=\{b,d\}} \mathbf{b}_\lambda^{(i)}(\tau)^\dagger \mathcal{G}_{0,\lambda\nu}^{(i)}(\tau - \tau')^{-1} \mathbf{b}_\nu^{(i)}(\tau') \\ & + \int_0^\beta d\tau \left\{ \sum_{\lambda,\nu} \frac{1}{2} U_{\lambda,\nu} n_\lambda^{(i)}(\tau) (n_\nu^{(i)}(\tau) - \delta_{\lambda\nu}) \right. \\ & \left. - \sum_{\langle ij \rangle, \nu} t_\nu (b_\nu^{(i)}(\tau)^* \phi_{j,\nu}^{(i)}(\tau) + b_\nu^{(i)}(\tau) \phi_{j,\nu}^{(i)}(\tau)^*) \right\} \end{aligned} \quad (2)$$

where i is the index of the lattice site. In this equation τ is imaginary time and the function $\mathcal{G}_{0,\lambda\nu}^{(i)}(\tau - \tau')$ is a local non-interacting propagator interpreted as a *local* dynamical Weiss mean-field and is determined in a self-consistent manner. Here we use the Nambu notation $\mathbf{b}_\nu^{(i)}(\tau) \equiv (b_\nu^{(i)}(\tau), b_\nu^{(i)}(\tau)^*)$. Moreover the static bosonic mean-fields are defined in terms of the bosonic operator $b_{j,\nu}$ as

$$\phi_{j,\nu}^{(i)}(\tau) = \langle b_{j,\nu} \rangle_0. \quad (3)$$

The index 0 indicates that all averages are taken for the cavity system *i.e.* excluding the impurity site. Now each of the local actions can be treated as an impurity in the presence of a bath (representing the influence of the rest of the lattice) and therefore captured via an Anderson impurity Hamiltonian. There are several techniques to solve the impurity model. Here we apply Exact Diagonalization (ED) [26].

In practice, we start with an initial set of local Weiss Green's functions and local bosonic superfluid order parameters $\phi_{j,\nu}^{(i)}(\tau)$. After solving the action (2), we obtain a set of local self-energies $\Sigma_{\lambda\nu}^{(i)}(i\omega_n)$ with ω_n being Matsubara frequency. Then we employ the Dyson equation in real-space representation in order to compute the interacting lattice Green's function

$$\mathbf{G}(i\omega_n)^{-1} = \mathbf{G}_0(i\omega_n)^{-1} - \Sigma(i\omega_n). \quad (4)$$

The site-dependence of the Green's functions is shown by boldface quantities that denote a matrix form with site-indexed elements. Here $\mathbf{G}_0(i\omega_n)^{-1}$ stands for the non-interacting Green's function

$$\mathbf{G}_0(i\omega_n)^{-1} = (\mu + i\omega_n)\mathbf{1} - \mathbf{t} - \mathbf{V}. \quad (5)$$

In this expression, the matrix elements t_{ij} are hopping amplitudes for a given lattice structure and the external potential is included via $V_{ij} = \delta_{ij}V_i$ with $V_i = V_0 r_i^2$ and r_i being the distance from the trap center. Eventually the self-consistency loop is closed by specifying the Weiss Green's function via the local Dyson equation

$$\left(\mathcal{G}_{0,\lambda\nu}^{(i)}(i\omega_n)\right)^{-1} = \left(\mathbf{G}_{\lambda\nu}^{(i)}(i\omega_n)\right)^{-1} + \Sigma_{\lambda\nu}^{(i)}(i\omega_n). \quad (6)$$

where the diagonal elements of the lattice Green's function yield the interacting local Green's function $\mathbf{G}_{\lambda\nu}^{(i)}(i\omega_n) = (\mathbf{G}_{\lambda,\nu}(i\omega_n))_{ii}$. This self-consistency loop is repeated until the desired accuracy for superfluid order parameters and Weiss Green function is obtained.

Complementary to RDBMFT, in this work we employ an LDA approach combined with single-site BDMFT to explore the physics of the model (1). Here we adjust the chemical potential on each lattice site according to LDA as $\mu_\nu(r) = \mu_\nu^0 - V(r)$. The advantage of this approach is the larger system size accessible. We validate it by comparison with the more rigorous RDBMFT approach. In this paper, we apply RDBMFT for 2D lattices and LDA+BDMFT both for 2D and 3D lattices.

III. MAGNETIC PHASES OF A HOMOGENEOUS BOSE-HUBBARD MODEL

We start by exploring the two-component Bose-Hubbard model in the homogeneous case. We consider a 3D cubic lattice and focus on the situation of total filling $n = n_b + n_d$ being $n = 1$ and $n = 2$ with balanced densities $n_b = n_d = 0.5$ and $n_b = n_d = 1$ respectively. For each filling, we calculate both zero and finite temperature phase diagrams. We focus on the interaction regime where the inter-species interactions, $U_{bb} \equiv U_b, U_{dd} \equiv U_d$, and intra-species interaction, U_{bd} , are just slightly different, *i.e.* $U_b = U_d = 1.01 U_{bd}$. This particular regime of interactions is accessible by Feshbach resonances, and indeed our choice is motivated by a recent experiment at MIT [22], where a sample of ^{87}Rb atoms in hyperfine states $|1, -1\rangle$ and $|2, -2\rangle$ with nearly equal inter- and intra-species interactions has been prepared. The selection of interactions (U_{bd} slightly smaller than $U_{b,d}$) is due to more novel magnetic phases appearing in this regime [12]. In all our calculations we set $U_{bd} = 1$ as the unit of energy, and z is the number of the nearest neighbors for each site.

Fig. 1 displays the zero and finite temperature phase diagrams of the system with a total filling of one particle per site, $n = 1$. At $T = 0$ (upper panel) we find three

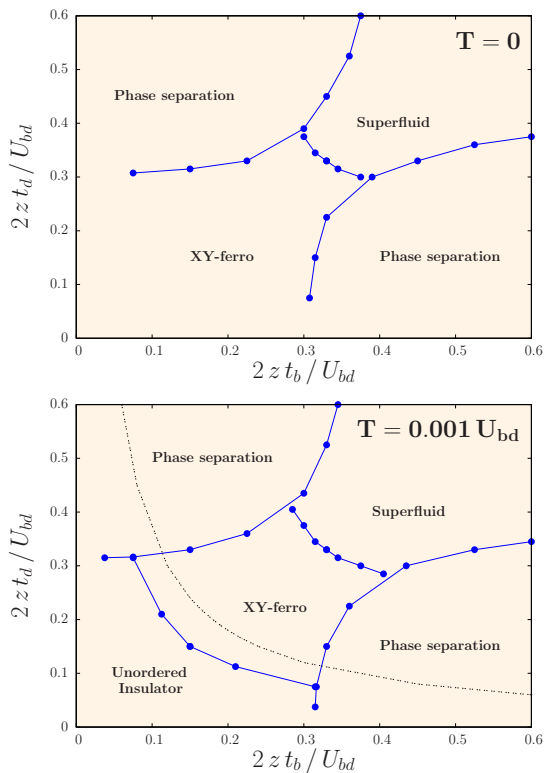


FIG. 1: Upper panel: zero-temperature phase diagram for the two-component Bose-Hubbard model in a 3D cubic lattice, as a function of hopping parameters. The interaction values are $U_b = U_d = 1.01 U_{bd}$ and the total filling is $n = 1$ with $n_b = n_d = 0.5$ (except in the phase separation regime). Lower panel: finite temperature phase diagram ($T = 0.001 U_{bd}$). The energy scale of the magnetic coupling $4t_b t_d / U_{bd}$ is shown by the black dashed line.

distinct phases which are characterized according to the value of the superfluid order parameters ϕ_b, ϕ_d and the two-body correlator $\phi_{bd} = \langle b d^\dagger \rangle - \langle b \rangle \langle d^\dagger \rangle > 0$ which indicates the XY-ferromagnetic spin-ordering. When both species have comparably large hopping, we find a superfluid phase characterized by $\phi_{b,d} \neq 0$. Instead when the hopping amplitudes are very different, the species with larger hopping is more easily delocalized and therefore superfluid, while the other component favors a Mott insulating phase. In this parameter regime, we do not find a homogeneous converged BDMFT solution where each component has the same filling, which indicates phase separation between the superfluid and the Mott insulator. We notice that the phase diagram is symmetric upon particle interchange and this symmetry is also manifested in the Hamiltonian (1). The third phase emerges when the hopping amplitudes are small. This non-superfluid (*i.e.* Mott insulating) phase possesses an XY-ferromagnetic spin-ordering and is characterized by $\phi_{b,d} = 0$ and $\phi_{bd} > 0$.

We investigate also the effect of finite temperature on the phase diagram as shown in the lower panel of Fig. 1.

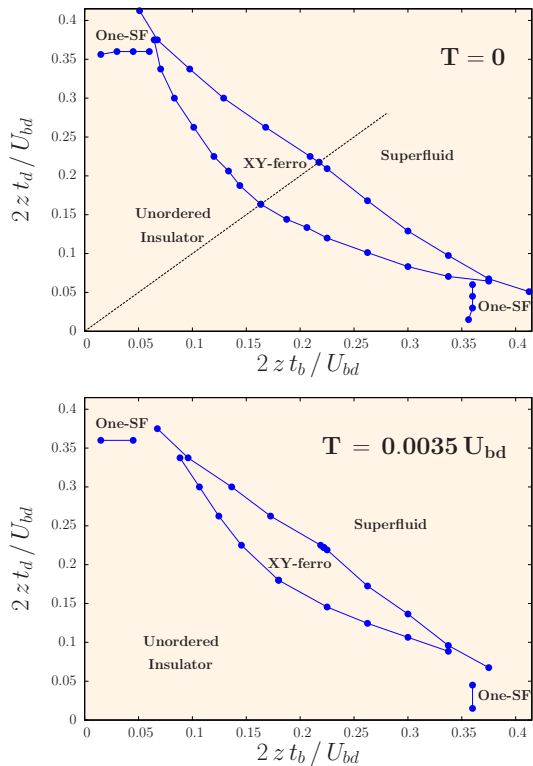


FIG. 2: Upper panel: zero-temperature phase diagram for a two-component Bose-Hubbard model in a 3D cubic lattice, as a function of hopping parameters. The diagonal dotted line shows $t_b = t_d$. The interaction values are $U_b = U_d = 1.01 U_{bd}$ and the total filling is 2 with $n_b = n_d = 1$. Lower panel: finite temperature phase diagram ($T = 0.0035 U_{bd}$).

We observe that the superfluid remains robust against small finite T . On the other hand, the XY-ferromagnetic spin-ordered phase is sensitive to finite temperature since it is formed in the low-hopping regime and therefore easily destroyed by thermal fluctuations. At finite T this ordered phase is reduced in favor of developing a non-magnetically ordered Mott state which is characterized by $\phi_{bd} = 0$ and $\phi_{b,d} = 0$ and which we denote as “unordered insulator” in the following. The black dashed line shows the energy scale of the magnetic coupling $4t_b t_d / U_{bd}$ [12].

Now we turn to the case when the total filling at each site is $n = 2$. Fig. 2 (upper panel) shows the zero-temperature phase diagram for this case. The main difference compared to $n = 1$ is the presence of a large unordered (Mott) insulator at low hopping values. As for $n = 1$, here we also find a sizable superfluid regime when both species have large hopping amplitudes. Instead, when the hopping amplitude for one component is very small and the other one very large, the system will be in a new phase with one component being superfluid and the other one Mott insulating. This *one-component superfluid* phase, *e.g.* for the d component, is defined

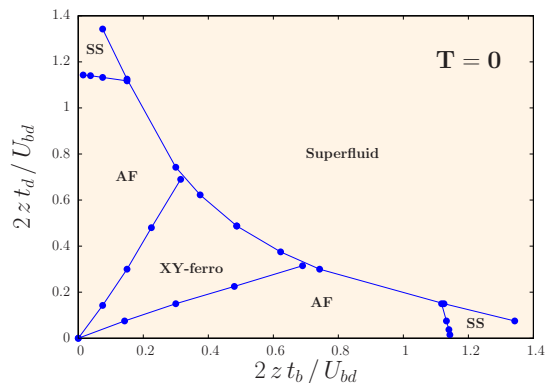


FIG. 3: Zero-temperature phase diagram for a two-component Bose-Hubbard model in a 3D cubic lattice, as a function of hopping parameters. The interaction values are $U_b = U_d = 12 U_{bd}$ and the total filling is $n = 1$ with $n_b = n_d = 0.5$.

by $\phi_b = 0$ and $\phi_d > 0$. There are also two Mott states: the XY-ferromagnet at intermediate hopping and the unordered (Mott) insulator in the lower hopping regime. At finite temperature (lower panel) both superfluid phases remain robust and almost unchanged. The main effect of finite T is to reduce the XY-ferromagnetic phase in favor of the unordered (Mott) insulator. The finite- T phase diagram of Fig. 2 is in remarkable agreement with the one obtained by a field-theoretical approach [14].

A further important spin-ordered state is the anti-ferromagnetic (AF) phase. Its existence in the Mott domain has been shown in previous investigations [11, 12]. In order to address this phase within our formalism, we adopt a set of parameters in which the inter-species interactions $U_{b,d}$ are much larger than the intra-species one: $U_b = U_d = 12 U_{bd}$. This specific choice is inspired by a previous BDMFT study [26] in which the phase diagram was obtained on the Bethe lattice. Here we aim to map out the phase diagram on a 3D cubic lattice which is directly relevant for the experimental studies. Fig. 3 sketches the phase diagram for this case with the total particle filling $n = 1$. In addition to two previously discussed phases, superfluid and XY-ferromagnet, (see Fig. 1, 2), we find two other ordered states here: AF phase and super-solid. For unequal hopping in the Mott domain, we identify a magnetically ordered phase of AF type. This non-superfluid phase (*i.e.* $\phi_{b,d} = 0$) is characterized by a finite value of the AF order parameter $\Delta_{AF}^\nu = |n_{\nu,\alpha} - n_{\nu,\bar{\alpha}}| > 0$, where ν denotes the component and α is the sublattice ($\bar{\alpha} = -\alpha$), together with vanishing XY-ferromagnetic order $\phi_{bd} = 0$. Finally for a very large difference in the hopping of the two species we observe a small window of a super-solid phase with $\phi_b > 0, \phi_d = 0$ and $\Delta_{AF} > 0$ if $t_b \gg t_d$, and vice versa.

To investigate in detail the quantum phase transition into the XY-ferromagnetically ordered state, for $n = 2$ and at $T = 0$, in Fig. 4 we plot the behavior of individ-

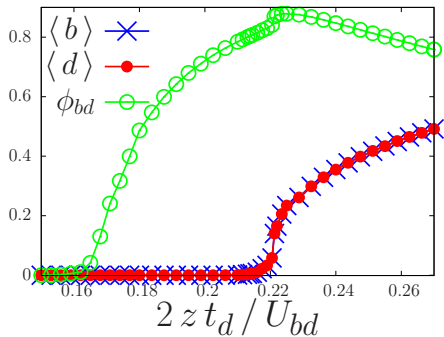


FIG. 4: t_d dependence of order parameters $\langle b \rangle$, $\langle d \rangle$, and ϕ_{bd} along the diagonal black dotted line in the upper panel of Fig. 2. The interaction regime is set to $U_b = U_d = 1.01 U_{bd}$ and the hopping amplitudes $t_b = t_d$ with filling factors $n_b = n_d = 1$.

ual superfluid order parameters and also the correlator ϕ_{bd} along the line of $t_b = t_d$ (the diagonal black dotted line shown in the upper panel of Fig. 2). The latter behavior indicates a second-order quantum phase transition from the Mott state to the XY-ferromagnet and also a second-order phase transition from XY-ferromagnet to superfluid.

One crucial question regarding observation of the AF and XY-ferromagnetic orders is how fragile they are against finite-temperature effects. To address this important issue, we compute the respective critical temperatures. Fig. 5 shows T_c as a function of the hopping amplitude of species b while we keep the hopping ratio fixed as $t_d = 4t_b$ for the AF phase (upper panel) and as $t_b = t_d$ for the XY-ferromagnetic phase (lower panel). We notice that T_c rises as the hopping amplitudes increase, due to the growing effective exchange couplings which stabilize magnetic order. We also note that the zero-temperature phase diagram on a 3D cubic lattice for filling $n = 1$, containing the AF phase (Fig. 3), has the same structure as the corresponding one on the Bethe lattice [26]. Therefore we anticipate that the finite- T counterpart of this phase diagram should also be similar on both lattices, and therefore expect there is a region of unordered Mott insulator at low hopping. The inset of Fig. 5 (upper panel) shows the temperature dependence of Δ_{AF}^{ν} . It indicates a second-order phase transition from the AF phase to the unordered Mott insulator. We have also computed the order parameter ϕ_{bd} for the XY-ferromagnetic phase as shown in the lower inset of Fig. 5 which indicates a 2nd order transition from the XY-ferromagnetic phase to an unordered Mott insulator as well. The critical temperatures of magnetic phases shown here are notably smaller than the coldest temperatures which have been measured in most experiments until now, apart from W. Ketterle's group where temperatures as low as 350 pK ($\approx 0.01 U_{bd}$) have been achieved [23].

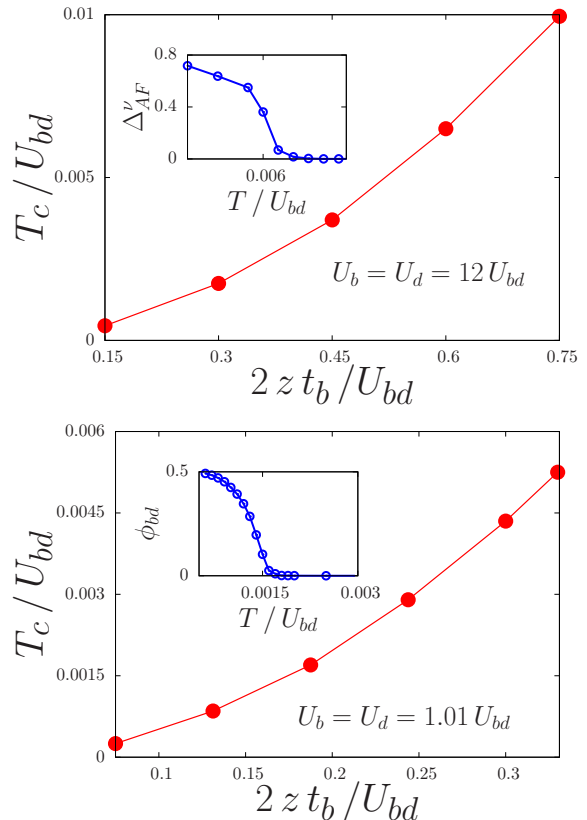


FIG. 5: Critical temperature of AF and XY-ferromagnetic order as a function of the hopping amplitude t_b on a 3D homogeneous cubic lattice with total filling $n = 1$. **Upper panel:** AF phase with hopping amplitude ratio $t_b = 4t_d$. Inset: melting of the AF phase vs temperature with hopping amplitudes $2zt_b = 0.6 U_{bd}$ and $2zt_d = 0.15 U_{bd}$. **Lower panel:** XY-ferromagnetic phase for equal hopping amplitudes $t_b = t_d$. Inset: melting of the XY-ferromagnetic phase vs temperature with hopping amplitudes $2zt_b = 2zt_d = 0.1875 U_{bd}$.

IV. SPIN-ORDERING FOR AN INHOMOGENEOUS BOSE-HUBBARD MODEL

In the previous section, we focused on homogeneous systems. However all the experiments are carried out in the presence of an external confining potential. Therefore we extend the BDMFT scheme to real-space BDMFT to address the inhomogeneous system. In this section, using RBDMFT and LDA+BDMFT, we will explore an inhomogeneous two-component Bose-Hubbard model both in 2D and 3D.

A. 2D trapped Bose gas

In this section we discuss the AF phase, the XY-ferromagnet and the unordered Mott state in a 2D square lattice in the presence of a harmonic trap. We first investigate AF ordering on a 31×31 lattice and then XY-

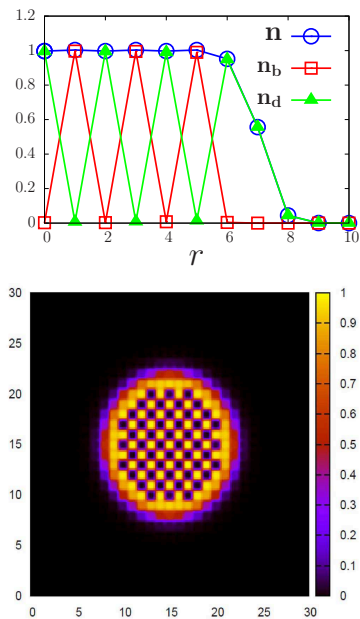


FIG. 6: Néel-type AF order in 2D at central filling $n = 1$ and $T = 0$. **Top:** particle densities of the two species as a function of radial distance r . The interactions are set to $U_b = U_d = 12 U_{bd}$, the hopping amplitudes $2zt_b = 0.1 U_{bd}$ and $2zt_d = 0.25 U_{bd}$ with harmonic trap $V_0 = 0.01 U_{bd}$. The chemical potentials are $\mu_b = \mu_d = 0.5 U_{bd}$. **Bottom:** density distribution of the d component over the lattice.

ferromagnetic phase and the unordered Mott state on a 32×32 lattice. The choice of different lattice sizes is solely due to computational convenience.

1. Anti-ferromagnet order

One of the most desirable goals in the current experiments on cold atomic-gases is to reach the regime of (Néel-type) AF ordering which is (for fermionic systems) expected to be a key step towards realizing a d -wave superfluid phase [6]. Here we investigate this phase for trapped two component bosons in an optical lattice. At the beginning we focus on AF order at $T = 0$. We choose the interaction parameters as $U_b = U_d = 12 U_{bd}$ with the unequal hopping for two species fixed as $2zt_b = 0.1 U_{bd}$ and $2zt_d = 0.25 U_{bd}$. We choose a maximum local filling of $n = 1$ at the center of the trap. The top panel of Fig. 6 shows the RBDMFT results for the particle densities as a function of radial distance r from the trap center. The AF phase forms in the central area of the lattice as a checker-board pattern and vanishes smoothly with increasing distance r from the lattice center. This indicates that AF order is stable at the center of a finite trap. However due to the unequal hopping, the lighter species (*i.e.* the one with the larger hopping) explores the lattice more freely and forms a superfluid ring around the

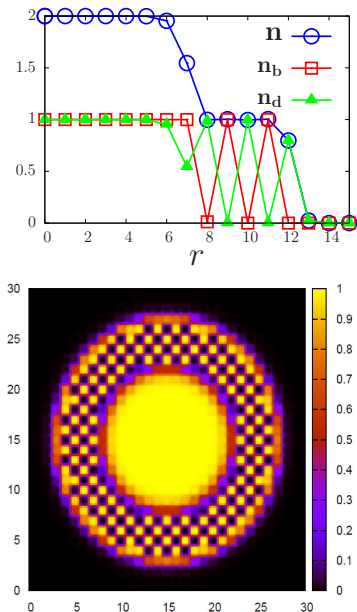


FIG. 7: Néel-type AF order in 2D at central filling $n = 2$ and $T = 0$. **Top:** particle densities of the two species versus radius obtained by RBDMFT. Interactions are set to $U_b = U_d = 48 U_{bd}$, the hopping amplitudes to $2zt_b = 0.1 U_{bd}$ and $2zt_d = 0.25 U_{bd}$, with a harmonic trap strength $V_0 = 0.01 U_{bd}$. The chemical potentials are $\mu_b = \mu_d = 1.5 U_{bd}$. **Bottom:** density distribution of the d component over the lattice.

central checker-board pattern. This behavior is visible in the bottom panel of Fig. 6. To see how robust AF order is against changing the total atom filling number, we now increase the filling at the center of the trap to $n = 2$, and observe that AF order now forms as a ring around the center as shown in Fig. 7. We conclude that also in 2D and in the presence of a trapping potential, AF order can be observed in regions of total filling $n = 1$ at $T = 0$.

2. XY-ferromagnet

As evident in the phase diagrams of the homogeneous system (Figs. 1, 2), a common magnetic phase which appears for both fillings $n = 1$ and $n = 2$ is the XY-ferromagnet. Here we investigate the stability of the XY-ferromagnetic phase in a trapped 2-component system on a 2D lattice of size 32×32 at $T = 0$. We first focus on the case of equal hopping $2zt_b = 2zt_d = 0.175 U_{bd}$ for both species and choose the interactions as $U_b = U_d = 1.01 U_{bd}$. In Fig. 8 the atom densities, their corresponding superfluid order parameters and the correlator ϕ_{bd} are shown as determined from RBDMFT (top panel) and LDA+BDMFT (lower panel). At the center of the lattice, we have a total filling of $n = 2$. We observe a finite value of the correlator ϕ_{bd} which implies a stable XY-ferromagnetic phase in this inhomogeneous system. With

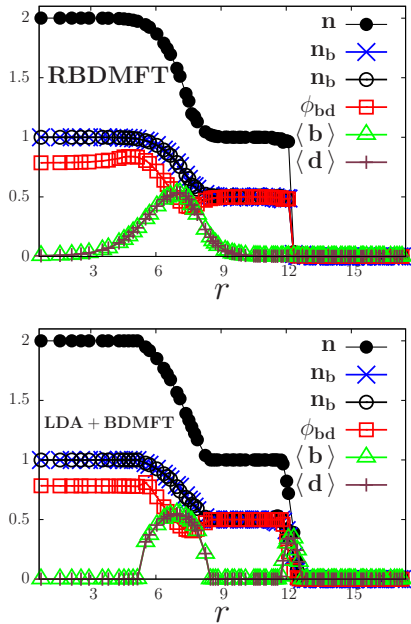


FIG. 8: Top: RBDMMFT results in 2D for atom densities, superfluid order parameters and XY-ferromagnetic correlator ϕ_{bd} as a function of radial distance r at $T = 0$. Interactions are set to $U_b = U_d = 1.01 U_{bd}$, with hopping amplitudes $2zt_b = 2zt_d = 0.175 U_{bd}$ and harmonic trap $V_0 = 0.01 U_{bd}$. The chemical potentials are $\mu_b = \mu_d = 1.5 U_{bd}$. Bottom: LDA+BDMFT results for the same parameters as the top panel.

increasing distance from the trap center, we find non-zero values for the superfluid order parameters with a maximum inside the atomic cloud, indicating the superfluidity for both species. We can also see that the correlator ϕ_{bd} remains finite in the superfluid regime. Moving further towards the edge of the trap, the XY-ferromagnetic phase with $n = 1$ appears and eventually a further superfluid domain. For comparison, we have computed the same quantities within LDA+BDMFT, which are shown in the bottom panel of Fig. 8. We find an excellent agreement between RBDMMFT and LDA+BDMFT deep inside each phase, but RBDMMFT provides the more accurate description of the smooth transition between the different phases. Note that the second superfluid ring is very narrow within RBDMMFT which is most likely a finite-size effect.

3. Unordered Mott state

We now consider the case of low hopping amplitudes. This situation corresponds to the regime of the large area of the unordered Mott state (without symmetry breaking) in the homogeneous phase diagram (see Figs. 1,2 for the 3D case). In Fig. 9 we show results for the atomic densities, superfluid order parameters, and the correlator

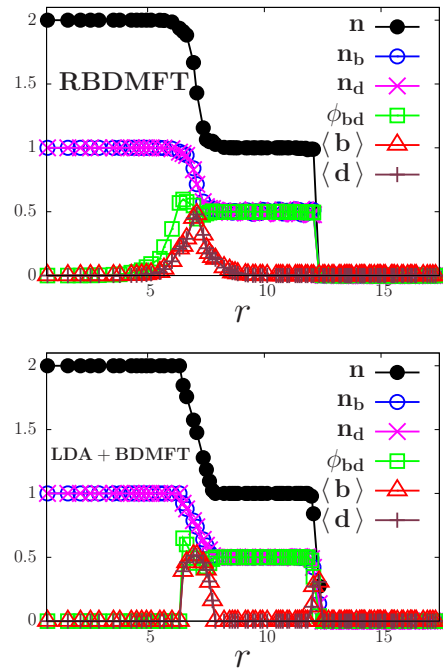


FIG. 9: Unordered Mott state in 2D at $n = 2$ for weak hopping amplitudes at $T = 0$, calculated by RBDMMFT (top panel) and LDA+BDMFT (bottom panel). The interactions and hopping amplitudes are $U_b = U_d = 1.01 U_{bd}$ and $2zt_b = 2zt_d = 0.1 U_{bd}$, with the harmonic trap $V_0 = 0.01 U_{bd}$. The chemical potentials are $\mu_b = \mu_d = 1.5 U_{bd}$.

for ϕ_{bd} for the case $2zt_b = 2zt_d = 0.1 U_{bd}$ at $T = 0$. In the center of the lattice where we have filling $n = 2$, the low-energy Hilbert space of each lattice site includes the three states $|b, b\rangle, |d, d\rangle$ and $|b, d\rangle$. With the choice of the interactions as $U_{b,d} > U_{bd}$, the third state has the lowest energy and therefore we have a Mott state with $\phi_{bd} = 0$ and no symmetry breaking. For intermediate radii, where $1 < n < 2$ and both species are superfluid, ϕ_{bd} rises to a finite value and remains constant in the $n = 1$ region where the XY-ferromagnet is stable.

B. 3D trapped case

In this final part, we consider the experimentally most interesting case of a 3D cubic optical lattice in the presence of an external harmonic trap. Due to the computational limitations for RBDMMFT, here we only apply LDA+BDMFT which we previously benchmarked versus RBDMMFT. Throughout this section, we consider a lattice with $41 \times 41 \times 41$ sites.

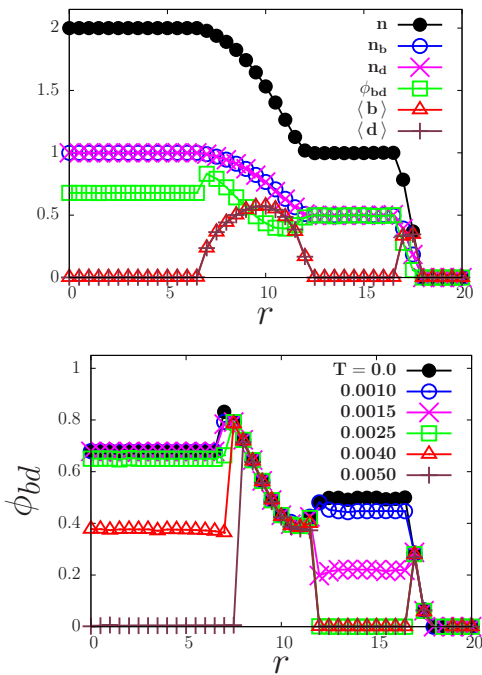


FIG. 10: Top: particle densities, superfluid order parameters and XY-ferromagnetic correlator as a function of radius r on a 3D cubic lattice at $T = 0$, calculated within LDA+BDMFT. Interactions are set to $U_b = U_d = 1.01 U_{bd}$, hopping amplitudes $2zt_b = 2zt_d = 0.195 U_{bd}$ with a harmonic trap $V_0 = 0.005 U_{bd}$ and $N_{tot} = 2.6 \times 10^4$. Bottom: Temperature dependence of the XY-ferromagnetic correlator for the same parameters as the top panel.

1. XY-ferromagnet

We begin the 3D trapped lattice analysis by investigating the stability of the XY-ferromagnetic phase. We first choose intermediate hopping as $2zt_b = 2zt_d = 0.195 U_{bd}$. This choice corresponds to the XY-ferromagnet in the homogeneous phase diagrams (Fig. 1,2). We enforce filling $n = 2$ at the center of the lattice by adopting the proper chemical potentials. In Fig. 10 (top panel) we show the particle densities, superfluid order parameters and the correlator ϕ_{bd} at $T = 0$ (top panel) and at finite T (bottom panel). For $T = 0$ we observe a wedding-cake structure of the atomic densities *i.e.* two plateaus of $n = 1$ and $n = 2$ and intermediate areas with non-integer filling. However we are more interested in the magnetic properties which are revealed by the correlator ϕ_{bd} . We observe that in the $n = 2$ domain, there is a XY-ferromagnetic phase, manifested by a finite value of ϕ_{bd} and vanishing superfluid order parameters. In the intermediate area $1 < n < 2$, we obtain a superfluid phase with both $\langle b \rangle$ and $\langle d \rangle$ being finite. Note that the onset of superfluidity leads to non-zero XY-ferromagnetic correlations as well. By approaching the second Mott plateau with $n = 1$, the superfluid order parameters vanish again

and we obtain a non-zero value for ϕ_{bd} , indicating once again an insulating XY-ferromagnet. Finally for $n < 1$ we find a further superfluid domain.

As in the previous section, we are interested in the effect of temperature on magnetic order. Fig. 10 (bottom panel) represents the correlator ϕ_{bd} for different temperatures. First we notice that for all the temperatures considered here, the correlator possesses a larger value at $n = 2$ compared to $n = 1$. In other words, XY-ferromagnetic order is more pronounced for $n = 2$ compared to $n = 1$ as long as all other parameters of the Bose-Hubbard model are identical. To make this point more clear, we calculate the critical temperature for ferromagnetic order for both $n = 1$ and $n = 2$, and find respectively $T_c = 0.0018 U_{bd}$ (≈ 70 pK) and $T_c = 0.0051 U_{bd}$ (≈ 190 nK). We also calculate the maximum value of the critical temperature for XY-ferromagnetic order at filling $n = 1$ and $n = 2$, and find that the maximum value of the critical temperature is around 200 pK and 230 pK, respectively, when the 3D cubic lattice is formed by laser beams of wave-length 1064 nm and the scattering length is around $100a_b$ (a_b is the Bohr radius). This fact could be significant for ongoing experiments, *e.g.* in Refs. [22, 23] where spin gradient thermometry has been used to measure temperatures as low as 350 pK in a 3D optical lattice. Our calculation here indicates that it is much easier to observe XY-ferromagnetism for higher filling due to the enhanced critical temperature.

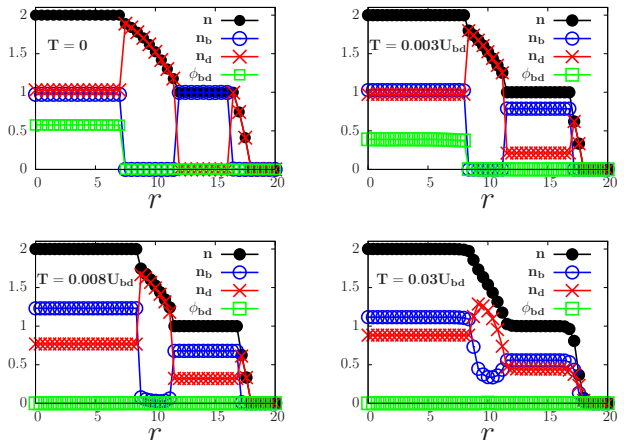


FIG. 11: Particle densities and XY-ferromagnetic correlator vs radial distance r for asymmetric hopping amplitudes $2zt_b = 0.15 U_{bd}$ and $2zt_d = 0.225 U_{bd}$ on a 3D cubic lattice. Interactions are $U_b = U_d = 1.01 U_{bd}$, the trapping potential is $V_0 = 0.005 U_{bd}$ and $N_{tot} = 2.6 \times 10^4$.

We now consider asymmetric values for the hopping amplitudes $2zt_b = 0.15 U_{bd}$ and $2zt_d = 0.225 U_{bd}$. By adjusting the chemical potentials, we obtain a globally almost balanced mixture with $N_b \simeq N_d \simeq (48\% - 52\%) N_{tot}$ with $N_{tot} = 2.6 \times 10^4$. Fig. 11 shows the atomic densities and XY-ferromagnetic spin-order for different temperatures (four panels). The most remarkable new feature of the asymmetric hopping regime is the vanishing ferro-

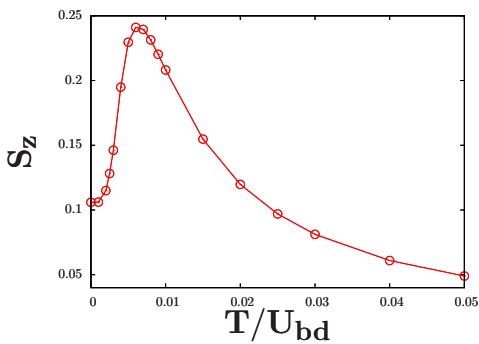


FIG. 12: Z-magnetization (imbalance) S_z vs temperature for the *homogeneous* system. Interactions are set to $U_b = U_d = 1.01 U_{bd}$ with hopping amplitudes $2zt_b = 0.15 U_{bd}$ and $2zt_d = 0.225 U_{bd}$ and total filling $n = 2$.

magnetic order in the $n = 1$ domain where $\phi_{bd} = 0$ even at $T = 0$. We also find that the total density profile first becomes sharper and then smoother again with increase of temperature. This is due to the higher spin entropy of the unordered two-component Mott insulator. Details will be discussed in a future publication [34].

It is visible in Fig. 11 that the lighter species (*i.e.* the one with larger hopping) always dominates the density distribution in the superfluid area where $n \neq 1, 2$, since in this regime the particle mobility plays a more important role than in the Mott domains. For the Mott state ($n = 1, 2$) the situation differs. In the spin model language [10–12], different hopping amplitudes lead to the existence of an effective magnetic field [10, 12],

$$h = z(2S + 1) \frac{t_b^2 - t_d^2}{U_{bd}} + \mu_b - \mu_d.$$

where $S = n/2$. This effective magnetic field gives rise to an imbalance between n_b and n_d which we quantify by the Z-magnetization $S_z = (n_b - n_d)/2$. At the Mott plateau with $n = 1$, the magnetization will shrink from $1/2$ (maximum of Z-magnetization due to a large effective magnetic field) to zero with increasing T due to thermal fluctuations. At the Mott plateau with $n = 2$, the magnetization depends non-monotonically on temperature. In Fig. 12, we show the temperature dependence of the magnetization at filling $n = 2$ plateau by focusing on the trap center and performing a finite- T study with a single-site BDMFT for the *homogeneous* model. This behavior can be understood if we notice that in the filling $n = 2$ region the system favors a state with a small magnetization S_z at zero temperature due to a non-zero effective magnetic field. Once the temperature starts to increase from zero to a finite value, thermal fluctuations will come into play and compete with quantum fluctuations, which makes the imbalance reach a maximum at finite T , since both types of fluctuations can delocalize the atoms and smooth the imbalance between the two species. When the temperature increases even higher,

the larger thermal fluctuations will simply smear out the imbalance.

2. Unordered Mott state

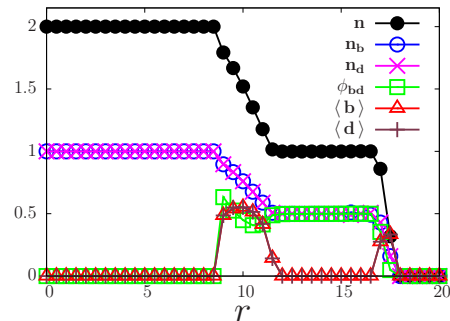


FIG. 13: Unordered Mott state at $n = 2$ for weak hopping amplitudes at $T = 0$, calculated within LDA+BDMFT. Interactions are $U_b = U_d = 1.01 U_{bd}$, hopping amplitudes $2zt_b = 2zt_d = 0.15 U_{bd}$, with a harmonic trap $V_0 = 0.005 U_{bd}$ and $N_{tot} = 2.6 \times 10^4$.

Finally, we also investigate the non-magnetic Mott state without symmetry breaking which occurs at $n = 2$ for relatively low hopping amplitudes $2zt_b = 2zt_d = 0.15 U_{bd}$ (see also the homogeneous phase diagrams Fig. 2). Fig. 13 (top panel) shows the results for atomic densities, their superfluid order parameters and the correlator ϕ_{bd} . At the center of the trap we indeed find a Mott state without symmetry breaking similar to the 2D case (Fig. 9).

V. SUMMARY AND OUTLOOK

In conclusion, we have studied magnetic ordering of a two-component Bose gas in 2D and 3D optical lattices. By using BDMFT we have calculated the phase diagrams of the homogeneous Bose-Hubbard model in a 3D cubic lattice with total particle filling $n = 1$ and $n = 2$, which feature superfluid and Mott-insulating phases and also notably reveal ordered phases with XY-ferromagnetism and Néel-antiferromagnetism in the Mott domain. We investigate the critical temperatures of these long-range ordered states. Moreover we have confirmed the stability of these magnetic phases in a trapped 2D or 3D system. In the case of a 3D cubic lattice, we have in particular computed XY-ferromagnetic ordering at finite temperatures which is relevant for current experiments [22, 23]. Another important issue is the detection of novel magnetic phases with long-range spin order. For an antiferromagnetic phase, spin-sensitive detection can be used to detect the Néel-type order, *i.e.* one spin component can be detected after removing the other one using

spin-selective single-site addressing, as pointed recently [35, 36]. For the XY-ferromagnetic phase, one could apply a $\pi/2$ pulse with a position-dependent phase (linear gradient), thus probing locally with different phases. For XY-ferromagnetic long-range order one would thus observe stripes with regular spacing when the phase matches and the $\pi/2$ pulse transfers all atoms into one of the two spin states [37].

Achieving the necessary ultra-low temperatures for detecting magnetic ordering of cold bosons in optical lattices has so far remained elusive. However, it is anticipated that by further experimental advances this obstacle will be overcome in the near future [38]. Our results

provide theoretical benchmarks which in the future will also be extended to other geometries such as triangular or hexagonal lattices.

Acknowledgments

We acknowledge useful discussions with S. Kuhr, I. Titvinidze, C. Weitenberg and D. Weld. This work was supported by the China Scholarship Fund (Y.L) and the Deutsche Forschungsgemeinschaft via SFB-TR 49, FOR 801 and the DIP project BL 574/10-1.

-
- [1] A. Auerbach, *Interacting electron and quantum magnetism*, Springer (1998).
- [2] S. Sachdev, *Nature Physics* **4**, 173 (2008).
- [3] M. Greiner, O. Mandel, T. Esslinger, T. W. Hänsch and I. Bloch, *Nature* **415**, 39 (2002).
- [4] S. Fölling, S. Trotzky, P. Cheinet, M. Feld, R. Saers, A. Widera, T. Müller and I. Bloch, *Nature* **448**, 1029 (2007).
- [5] S. Trotzky, P. Cheinet, S. Fölling, M. Field, U. Schnorrberger, A.M. Rey, A. Polovnikov, E.A. Demler, M.D. Lukin and I. Bloch, *Science* **319**, 295 (2008).
- [6] T. Esslinger, *Annual Review of Condensed Matter Physics* **1**, 129 (2010) (e-print arXiv:1007.0012).
- [7] W.S. Bakr, J.I. Gillen, A. Peng, S. Foelling and M. Greiner, *Nature* **462**, 74 (2009).
- [8] J.F. Sherson, C. Weitenberg, M. Endres, M. Cheneau, I. Bloch, S. Kuhr, *Nature* **467**, 68 (2010).
- [9] J. Simon, W.S. Bakr, R. Ma, M.E. Tai, P.M. Preiss and M. Greiner, *Nature* **472**, 307 (2011).
- [10] A. B. Kuklov and B. V. Svistunov, *Phys. Rev. Lett.* **90**, 100401 (2003).
- [11] L.-M. Duan, E. Demler, and M. D. Lukin, *Phys. Rev. Lett.* **91**, 090402 (2003).
- [12] E. Altman, W. Hofstetter, E. Demler and M. Lukin, *New Journal of Physics* **5**, 113 (2003).
- [13] S.G. Söyler, B. Capogrosso-Sansone, N.V. Prokof'ev, B.V. Svistunov, *New J. Phys.* **11**, 073036 (2009).
- [14] S. Powell, *Phys. Rev. A* **79**, 053614 (2009).
- [15] B. Capogrosso-Sansone, S.G. Söyler, N.V. Prokof'ev and B.V. Svistunov, *Phys. Rev. A* **81**, 053622 (2010).
- [16] L. de Forges de Parny, M. Traynard, F. Hébert, V.G. Rousseau, R.T. Scalettar, G.G. Batrouni, *Phys. Rev. A* **82**, 063602 (2010).
- [17] T. Barthel, C. Kasztelan, I. P. McCulloch and U. Schollwöck, *Phys. Rev. A* **79**, 053627 (2009).
- [18] K. Noda, A. Koga, N. Kawakami and T. Pruschke, *Phys. Rev. A* **80**, 063622 (2009).
- [19] U. Shrestha, *Phys. Rev. A* **82**, 041603 (2010).
- [20] J. Catani, L. Desarlo, G. Baronitini, F. Minardi and M. Inguscio, *Phys. Rev. A* **77**, 011603(R) (2008).
- [21] J. Catani, G. Barontini, G. Lamporesi, F. Rabatti, G. Thalhammer, F. Minardi, S. Stringari, and M. Inguscio, *Phys. Rev. Lett.* **103**, 140401 (2009).
- [22] D.M. Weld, P. Medley, H. Miyake, D. Hucul, D. E. Pritchard, and W. Ketterle, *Phys. Rev. Lett.* **103**, 245301 (2009).
- [23] P. Medley, D.M. Weld, H. Miyake, D.E. Pritchard and W. Ketterle, arXiv:1006.4674.
- [24] B. Gadway, D. Pertot, R. Reimann and D. Schneble, *Phys. Rev. Lett.* **105**, 045303 (2010).
- [25] K. Byczuk and D. Vollhardt, *Phys. Rev. B* **77**, 235106 (2008).
- [26] A. Hubener, M. Snoek and W. Hofstetter, *Phys. Rev. B* **80**, 245109 (2009).
- [27] W. Hu and N. Tong, *Phys. Rev. B* **80**, 245110 (2009).
- [28] M. Snoek and W. Hofstetter, arXiv:1007.5223.
- [29] P. Anders, E. Gull, L. Pollet, M. Troyer and P. Werner *Phys. Rev. Lett.* **105**, 096402 (2010).
- [30] W. Metzner and D. Vollhardt, *Phys. Rev. Lett.* **62**, 324 (1989).
- [31] A. Georges, G. Kotliar, W. Krauth and M. Rozenberg, *Rev. of Mod. Phys.* **68**, 12 (1996).
- [32] M. Snoek, I. Titvinidze, C. Toke, K. Byczuk and W. Hofstetter, *New J. Phys.* **10**, 093008 (2008).
- [33] R.W. Helmes, T.A. Costi and A. Rosch, *Phys. Rev. Lett.* **100**, 056403 (2008).
- [34] Y. Li *et al.*, in preparation.
- [35] C. Weitenberg, M. Endres, J. F. Sherson, M. Cheneau, P. Schauß, T. Fukuhara, I. Bloch, and S. Kuhr, *Nature* **471**, 319 (2011).
- [36] C. Weitenberg, P. Schauß, T. Fukuhara, M. Cheneau, M. Endres, I. Bloch, S. Kuhr, arXiv:1102.3859.
- [37] Private communication with Stefan Kuhr.
- [38] D. McKay and B. DeMarco, *Rep. Prog. Phys.* **74**, 054401 (2011).